Supplementary Material

Journal name: Cognitive Neurodynamics

Article title: Computational modeling of the fast-to-slow EEG rhythm transition across seizure evolution and postictal recovery

Feng Zhang[1], Meili Lu[2], Xile Wei[1]

[1]Tianjin Key Laboratory of Process Measurement and Control, School of Electrical and Information Engineering, Tianjin University, Tianjin, 300072, China

[2]School of Information Technology Engineering, Tianjin University of Technology and Education, Tianjin, 300222, China

Corresponding author: Xile Wei (xilewei@tju.edu.cn)

This supplementary material includes:

Section S1. Stochastic formulation and numerical implementation of the DCE model

Section S2. Extended clinical EEG analysis

Section S3. Component and coupling contributions

Section S4. Comparison of seizure-like events generated by the DCE and Epileptor models

References

Supplementary Figures S1-S5

Supplementary Tables S1-S5

Section S1. Stochastic formulation and numerical implementation of the DCE model

Auxiliary-state implementation of the filtering term

For numerical integration, we implement the exponential low-pass filtering in Eq. (10) through a first-order differential equation and evaluate the effective drive as follows:

$$\frac{du}{dt} = -\gamma(t)[u - 0.1x_1], \qquad p = 3.39z_1 - 6.46 + 25u. \tag{S1}$$

Here, u is an auxiliary filtering state that stores the filtered contribution of x_1. The filtering rate $\gamma(t)$ is selected according to the direction of the ultraslow variable z_1:

$$\gamma(t) = \begin{cases} \gamma_1, & \dot{z}_1 \geq 0, \\ \gamma_2, & \dot{z}_1 < 0. \end{cases} \tag{S2}$$

When the filtering rate switches between γ_1 and γ_2, u evolves continuously from its current value rather than being reinitialized. Introducing this auxiliary state extends the six core DCE variables to the seven-dimensional numerical state vector:

$$\mathbf{X} = (x_1, y_1, z_1, x_2, y_2, z_2, u)^{\mathrm{T}}. \tag{S3}$$

Additive stochastic formulation

Let F_{x_1}, F_{y_1}, F_{z_1}, F_{x_2}, F_{y_2}, F_{z_2}, and F_u denote the deterministic drift terms in the corresponding state equations, with p evaluated from Eq. (S1). The stochastic system used in the simulations is given by Eq. (S4).

$$\begin{cases} dx_1 = F_{x_1}(\mathbf{X})dt + \sigma_{\mathrm{I}} dW_{x_1}, \\ dy_1 = F_{y_1}(\mathbf{X})dt + \sigma_{\mathrm{I}} dW_{y_1}, \\ dz_1 = F_{z_1}(\mathbf{X})dt, \\ dx_2 = F_{x_2}(\mathbf{X})dt + \sigma_{\mathrm{II}} dW_{x_2}, \\ dy_2 = F_{y_2}(\mathbf{X})dt + \sigma_{\mathrm{II}} dW_{y_2}, \\ dz_2 = F_{z_2}(\mathbf{X})dt + \sigma_{z_2} dW_{z_2}, \\ du = F_u(\mathbf{X})dt. \end{cases} \tag{S4}$$

Here, W_{x_1}, W_{y_1}, W_{x_2}, W_{y_2}, and W_{z_2} are mutually independent standard Wiener processes. The Wiener terms enter the state equations directly as process noise; no noise is added post hoc to the simulated EEG output. A common diffusion amplitude is used for x_1 and y_1, and a separate common amplitude is used for x_2 and y_2. The variables z_1 and u receive no direct Wiener increments.

The diffusion intensities were set to ${\sigma_{\mathrm{I}}}^2 = 0.0001$, ${\sigma_{\mathrm{II}}}^2 = 0.0015$, and ${\sigma_{z_2}}^2 = 0.00004$. Accordingly, the diffusion amplitudes in Eq. (S4) are $\sigma_{\mathrm{I}} = \sqrt{0.0001}$, $\sigma_{\mathrm{II}} = \sqrt{0.0015}$, and $\sigma_{z_2} = \sqrt{0.00004}$.

Numerical integration

All seven numerical states were advanced jointly using a fixed integration step $\boldsymbol{h = 0.025}$ in dimensionless model time. At each step, the deterministic drift was approximated using the classical fourth-order Runge--Kutta method. The four stages were defined as

$$\begin{aligned}
\mathbf{k}_1 &= \mathbf{F}(t_n, \mathbf{X}_n), \\
\mathbf{k}_2 &= \mathbf{F}\left(t_n + \frac{h}{2}, \mathbf{X}_n + \frac{h}{2}\mathbf{k}_1\right), \\
\mathbf{k}_3 &= \mathbf{F}\left(t_n + \frac{h}{2}, \mathbf{X}_n + \frac{h}{2}\mathbf{k}_2\right), \\
\mathbf{k}_4 &= \mathbf{F}(t_n + h, \mathbf{X}_n + h\mathbf{k}_3).
\end{aligned}$$

where $\mathbf{F}$ denotes the deterministic drift vector. The additive Wiener increment was applied once after the deterministic Runge--Kutta update, yielding Eq. (S5). At each RK4 stage, the effective drive p and filtering rate γ are evaluated from the corresponding intermediate state.

$$\mathbf{X}_{n+1} = \mathbf{X}_n + \frac{h}{6}(\mathbf{k}_1 + 2\mathbf{k}_2 + 2\mathbf{k}_3 + \mathbf{k}_4) + \boldsymbol{\Sigma}\sqrt{h}\boldsymbol{\xi}_n, \quad \boldsymbol{\xi}_n \sim \mathrm{N}(0, \mathbf{I}). \tag{S5}$$

Here, $\boldsymbol{\Sigma} = \mathrm{diag}\left(\sigma_{\mathrm{I}}, \sigma_{\mathrm{I}}, 0, \sigma_{\mathrm{II}}, \sigma_{\mathrm{II}}, \sigma_{z_2}, 0\right)$, and $\boldsymbol{\xi}_n \sim \mathcal{N}(0, \mathbf{I})$. The standard normal vectors are sampled independently at each integration step. Because $\boldsymbol{\Sigma}$ is constant, the stochastic increment is state-independent and is evaluated once per integration step. All states are therefore advanced using a single scheme combining an RK4 drift update with an additive Wiener increment in Euler--Maruyama form.

Section S2. Extended clinical EEG analysis

S2.1 Dataset, acquisition, and analysis cohort

The Siena Scalp EEG Database comprises 47 annotated seizures from 14 patients (Table S1) recorded at the Unit of Neurology and Neurophysiology, University of Siena. According to the database documentation [1], video-EEG was acquired at 512 Hz with electrodes arranged according to the international 10-20 system, using EB Neuro or Natus Quantum LTM amplifiers and reusable silver/gold cup electrodes. The expert-provided patient-specific lists identify the EEG channels and the annotated seizure onset and offset times used in this analysis.

EDF signals were read in their stored physical units. Only channels identified as EEG in the patient-specific lists were considered; EKG and unlisted channels were excluded. The archived EEG was analyzed without additional filtering, re-referencing, detrending, resampling, or manual artifact rejection. The available dataset documentation does not specify a common recording reference or the acquisition filters' orders and transfer functions.

Definition of the 2-30 Hz analysis range

Inspection of the EDF metadata showed that acquisition filter settings varied across recordings, but that most nominal passbands covered 2-30 Hz. We therefore adopted 2-30 Hz as a harmonized frequency range for cross-patient spectral analysis. This range specifies which spectral bins enter the feature calculations; it is not an additional time-domain band-pass filter.

Before feature calculation, an event was eligible if its EDF channel metadata reported a nominal high-pass cutoff below 2 Hz and a nominal low-pass cutoff at or above 30 Hz (Table S2). Channels not meeting the same criterion were omitted. Of the 47 candidate seizures, 33 seizures from 11 patients were eligible. Fourteen seizures were excluded because their nominal passbands did not cover 2-30 Hz. One PN10 file contained a single incompatible channel; its three seizures were retained using the remaining 18 compatible EEG channels. This criterion provides a common analysis range spanning activity from the upper delta range to the beta band.

S2.2 Spectral feature extraction and trajectory analysis

For a seizure with annotated ictal duration D, the analysis window extended from seizure onset through D seconds after seizure offset. The STFT used a 512-sample periodic Hamming window, 410-sample overlap, and a 1024-point Fourier transform at 512 Hz. The CWT used generalized Morse wavelets with a time-bandwidth product of 60 and 10 voices per octave. Let $P(f,t)$ denote the linear spectral power at frequency f and time t. For the CWT, $P(f,t)$ was the squared magnitude of the wavelet coefficient; for the STFT, it was the power spectral density. Where available, 10 s of recorded EEG context on each side of the target interval was included when evaluating the transforms; only the target interval was retained for feature analysis.

At each time point, spectral centroid (SC), median frequency (MF), low-frequency ratio (LFR), and dominant frequency (DF) were defined as follows (evaluated over 2-30 Hz):

$$\mathrm{SC}(t) = \frac{\int_2^{30} fP\,(f,t)\mathrm{d}f}{\int_2^{30} P\,(f,t)\mathrm{d}f} \tag{S6}$$

$$\int_2^{\mathrm{MF}(t)} P\,(f,t)\mathrm{d}f = \frac{1}{2}\int_2^{30} P\,(f,t)\mathrm{d}f \tag{S7}$$

$$\mathrm{LFR}(t) = \frac{\int_2^{8} P\,(f,t)\mathrm{d}f}{\int_2^{30} P\,(f,t)\mathrm{d}f} \tag{S8}$$

$$\mathrm{DF}(t) = \underset{2\le f\le 30}{\arg\max}\, P(f,t) \tag{S9}$$

$$B_{[a,b]}(t) = \int_a^b P_{\mathrm{STFT}}\,(f,t)\mathrm{d}f, \qquad B_{\mathrm{dB}}(t) = 10\log_{10}\left(\frac{B_{[a,b]}}{1\mu\mathrm{V}^2}\right) \tag{S10}$$

$$B_{[a,b]}^{CWT}(t) = \frac{2}{C_\psi}\int_a^b \frac{|W(f,t)|^2}{f}\,df \tag{S11}$$

Under Eq. (S6), SC is the power-weighted mean frequency. MF was taken as the first ascending frequency whose cumulative power reached one half of the total. LFR quantifies the recorded 2-8 Hz delta/theta contribution within the analyzed 2-30 Hz portion of the delta-to-beta range. Absolute STFT power in Eq. (S10) and absolute CWT power in Eq. (S11) were evaluated for [a,b] = [2,8], [8,30], and [2,30] Hz.

For Eqs. (S6)-(S10), frequency integrals were evaluated using trapezoidal quadrature on the actual frequency grid in Hz, including its nonuniform spacing for the CWT. Cumulative power for MF was evaluated on the same ascending grid; DF was the frequency bin with the largest linear power.

Absolute CWT band power was calculated using Eq. (S11) [2], where W(f,t) denotes the L1-normalized analytic Morse coefficient of EEG recorded in microvolts. The integration measure df/f and normalization factor $2/C\psi$ yield band power in μV^2. The wavelet admissibility constant is $C\psi = 0.92102864$ for $\gamma = 3$ and $\beta = 20$, corresponding to a time-bandwidth product of 60. Trapezoidal integration in log frequency used coefficients spanning 1-60 Hz, with interpolated boundaries for the reported 2-8, 8-30, and 2-30 Hz bands. This scale weighting differs from that used for the relative CWT descriptors in Eqs. (S6)-(S9). Band power was converted to dB relative to 1 μV^2 before channel aggregation and averaging across seizures.

CWT SC and LFR were smoothed using a 256-sample Gaussian window (0.5 s), while MF and DF used a 256-sample moving median. STFT descriptors used five-frame windows (approximately 1 s), with Gaussian smoothing for SC and LFR and moving-median filtering for MF.

For comparisons across seizures, each channel-level feature trajectory was linearly interpolated onto 201 event-relative points spanning normalized time 0-2. Seizure onset, seizure offset, and the end of the matched postictal interval corresponded to 0, 1, and 2, respectively. At each time point, the median across eligible channels defined the seizure trajectory. Seizure trajectories were averaged within patients, with equal patient weighting in the cohort analysis. Early ictal (EI), late ictal (LI), and early postictal (EP) windows were defined as normalized times 0.10-0.40, 0.70-1.00, and 1.00-1.30, respectively. Phase changes were calculated as LI-minus-EI and EP-minus-EI window-mean differences. Least-squares slopes were fitted over normalized time 0-1 for ictal slopes and 0-2 for full-window slopes.

S2.3 Within-patient results for PN00

Four of the five annotated PN00 seizures met the harmonized passband criterion. Each event has negative CWT SC and MF ictal slopes and a positive LFR slope. The same directions hold for their full-window slopes. Each also has lower SC and MF and higher LFR in the early postictal than in the early ictal window (Table S3). These phase-window contrasts indicate greater relative low-frequency weighting during early postictal recovery than in the early ictal window. Figure 3(a-c) shows the individual trajectories and their mean, including the pronounced transient postictal rebound in Seizure 2. Figure 3(d-f) shows absolute CWT power in the same events. In all four, 2-8 Hz power rises more in dB than 8-30 Hz power from the early to the late ictal window. Both bands and total power decline from the late ictal to the early postictal window, while early postictal 2-8 Hz power remains above its early ictal level. The PN00 recordings thus show recurrent ictal rhythm slowing, with relative low-frequency weighting retained during early postictal recovery. Complementary analyses are presented in Section S2.4.

S2.4 Additional spectral analyses in PN00

Dominant frequency and spectral centroid

To further characterize spectral evolution, we examined dominant frequency (DF), the frequency with the highest spectral power at each time point, alongside SC (Figure S1). DF tracks the strongest spectral peak and can change abruptly when competing peaks exchange prominence, whereas SC summarizes the power-weighted frequency distribution.

In T5 and O2, DF frequently lies at the low-frequency end of the analyzed band, with intermittent higher-frequency excursions. A low-frequency spectral peak can therefore coexist with a higher SC because SC also reflects power elsewhere in the band. At the event level (Figure S1(c-f)), all four PN00 seizures have negative ictal DF slopes. Their late-ictal and early-postictal DF window means are also lower than their early-ictal means (Table S3). These directions agree with the SC, MF, and LFR changes in main-text Figure 3(a-c).

CWT and STFT comparisons

Figure S2 compares CWT- and STFT-derived SC trajectories for the two illustrative electrodes and all four PN00 events. Despite differences in absolute SC values and local fluctuations, the trajectories have broadly similar temporal profiles and provide consistent qualitative descriptions of spectral evolution. Both methods yield negative ictal SC slopes and lower early-postictal than early-ictal SC values in every PN00 event. These shared directions support ictal slowing and retained relative low-frequency weighting in the analyzed PN00 recordings.

S2.5 Extended cohort analysis

We extended the PN00 analysis in main-text Section 3.1 to 33 seizures from 11 patients meeting the common acquisition-passband criterion. In PN00, ictal slowing was reflected by negative SC and MF slopes and positive LFR slopes (Section S2.3 and Table S3). At the patient level, negative CWT-derived ictal slopes occurred in 7/11 patients for SC and 6/11 for MF, while LFR slopes were positive in 7/11. For STFT, the corresponding directions occurred in 7/11 patients for each descriptor (Table S4).

Postictal phase-window contrasts differed from the PN00 pattern. In PN00, early-postictal SC and MF remained below early-ictal values, while LFR remained higher. In the extended cohort, early-postictal SC and MF were higher than early-ictal values in 8/11 patients with CWT and 7/11 with STFT. LFR was lower in 8/11 patients with CWT and 7/11 with STFT (Table S4). These descriptive contrasts document variability in whether relative low-frequency weighting persisted into early postictal recovery. No SC, MF, or LFR endpoint reached a Benjamini-Hochberg-adjusted P value below 0.05 (Q column in Table S4).

Each measure was evaluated using four patient-level endpoints: the ictal least-squares slope, late-minus-early ictal change, early-postictal-minus-early-ictal change, and full-window slope. Two-sided exact Wilcoxon signed-rank tests used patients as the inferential units (n = 11). Benjamini-Hochberg correction was applied across the complete family of 52 exploratory tests. For each endpoint, a 95% confidence interval for the patient-level median was estimated using 10,000 patient-level bootstrap resamples. The family comprises four CWT descriptors, three STFT descriptors, and three absolute-power bands for each transform, each evaluated at the four endpoints. Table S4 reports all 52 comparisons under the same correction.

Taken together, the PN00 results illustrate ictal slowing followed by retained relative low-frequency weighting during early postictal recovery. The multi-patient analysis documents ictal slowing beyond PN00 and qualifies this within-patient pattern by showing variability in early postictal spectral evolution. Accordingly, the empirical conclusion in main-text Section 3.1 concerns a clinically observed pattern whose expression varies across seizures and patients. This motivates using the DCE model to investigate how interactions between fast and slow processes generate the fast-to-slow rhythm transition and shape its variability.

Section S3. Component and coupling contributions in the DCE model

The two components of the DCE model are Subsystems I and II. We first examine their waveforms and interaction across the model-defined interictal, ictal, and postictal periods, then analyze the underlying coupling mechanisms using controlled deterministic comparisons.

S3.1 Waveform evolution and subsystem contributions

Figure S3(a1-a4) shows the simulated EEG together with z_1, p, x_1, and x_2, using the same model, initial state, noise settings, and random-number state as main-text Figure 4(a). Subsystem I contributes rapid ictal-like oscillations and ultraslow modulation of recurrent events, whereas Subsystem II contributes spike, SWD, and slow-wave activity. The shaded intervals follow the phase boundaries in main-text Figure 4(a). Panel (a2) displays p and its oscillatory-regime thresholds alongside z_1, relating the waveform sequence to the model-defined phases.

The complete interictal interval following the first event contains low-amplitude background fluctuations and isolated spike-like events (Figure S3(b)). During the ictal period, prominent fast activity evolves into mixed fast and slower waveforms (Figure S3(c1)). The aligned 5-s EEG, x_2, and x_1 traces show that elevated portions of the slower x_2 cycles coincide with attenuation of the fast x_1 oscillations (Figure S3(c2-c4)), illustrating the modulation of the fast-component amplitude envelope. The postictal overview contains slow activity followed by transient spike-like activity during recovery (Figure S3(d1)). These features are illustrated in 10-s and 8-s windows, respectively (Figure S3(d2,d3)); the spike-dominated window lies within the spike regime as p declines.

The EEG readout $x_1 + 2x_2$ is displayed after fourth-order Butterworth 0.1-255 Hz forward-backward filtering, consistent with main-text Figure 4; the state-variable traces are unfiltered. The readout captures qualitative spectrotemporal organization, with amplitude in arbitrary units rather than calibrated microvolts; detailed waveform morphology has not been fitted to clinical EEG. Section S3.2 examines the coupling mechanisms underlying these component interactions.

S3.2 Controlled analysis of the coupling mechanisms

The controls in Figure S5 use noise-free dynamics and the default parameters in Table 1 of the main text, except for the stated control settings.

Subsystem I and ultraslow modulation. With the original cubic nonlinearity $f_1 = {x_1}^3 - 3{x_1}^2$, Subsystem I generates autonomous bursts under ultraslow z_1 modulation (Figure S5(a1)). For the coupled form, x_2 is fixed at 0.30 to examine how the periodic-orbit amplitude changes with z_1 while the x_2 input is held constant (Figure S5(a2)). The positive-branch modification produces a contracting amplitude envelope as z_1 increases.

Fixed-input fast-subsystem controls. To examine the x_2-dependent modulation, z_1 is instead fixed at 3. The (x_1, y_1) subsystem is compared using the original cubic form and the coupled form at $x_2 = 0.05$, 0.40, and 0.60. The peak-to-peak amplitudes are evaluated after convergence. Increasing the fixed feedback level contracts the limit cycle and ultimately produces convergence to equilibrium (Figure S5(b1-b4) and Table S5). The results in Figure S5(b2-b4) provide a dynamical explanation for the x_2-dependent modulation of the x_1 oscillation envelope observed in Figure S3(c3,c4). These two sets of controls distinguish the effects of the z_1 and x_2 inputs to the coupling function by holding one fixed while varying the other.

Isolated Subsystem II. With p held as a control parameter, the bifurcation diagram separates the non-oscillatory, spike, SWD, and wave regimes at $p = 0.43$, 3.03, and 5.12 (Figure S5(c)). The fast pair (x_2, y_2) and slow feedback z_2 supply separate spike and wave timescales. A fixed p selects a regime, whereas the evolving effective drive $p = f_2(x_1, z_1)$ in the full model organizes the progression through these regimes.

Removal of the filtered x_1 contribution. In the full model, $p = 3.39z_1 - 6.46 + 25u$, where u is defined in Section S1. In the comparison, the coefficient of u is set to zero, giving $p = 3.39z_1 - 6.46$. This removes the filtered pathway, not the direct z_1 dependence or the feedback through f_1. As shown in Figure S5(d), p ranges from -0.192 to 6.214 in the full model and from 3.363 to 7.404 when the filtered contribution is removed. The latter range remains above the SWD threshold, and Subsystem II continues to oscillate between bursts instead of entering the non-oscillatory regime. The filtered pathway is therefore required for access to the lower-p regimes and inter-event quiescence in this comparison, with the remaining equations and parameter values unchanged.

The stochastic trajectories display the complementary contributions of the two components, while the deterministic controls explain how their coupling coordinates waveform evolution, amplitude modulation, and access to the inter-event non-oscillatory regime. Together, these results establish the functional roles of the two subsystems and the filtered drive in the tested model configuration.

Section S4. Comparison of seizure-like events generated by the DCE and Epileptor models

In this section, we compare the simulated EEG generated by the Epileptor model proposed in [3] and the DCE model proposed in our study, to highlight their dynamical differences.

Figure S4(a,b) shows representative seizure-like events generated by the Epileptor model and the DCE model, respectively, together with their CWT spectrograms. In the tested parameter configuration, the Epileptor produces stereotyped spike-like discharges with a comparatively stable repetition frequency (panel (a1)), yielding a relatively stationary spectral structure with limited systematic spectral evolution during the seizure-like event (panel (a2)). In contrast, the DCE model exhibits a structured progression from fast ictal-like discharges to spike-like and spike-wave activity, followed by slow-wave oscillations (panel (b1)). This waveform evolution progressively shifts spectral power toward lower frequencies across the model-defined ictal and postictal periods (panel (b2)), qualitatively resembling the illustrative clinical spectral trajectory shown in Fig. 2(c) of the main text. This comparison suggests that the DCE model incorporates additional dynamical mechanisms for organizing spectral evolution during a seizure-like event. The comparison is intended to illustrate a qualitative dynamical difference rather than establish a quantitative goodness-of-fit advantage over the Epileptor.

References

[1] Detti P (2020) Siena Scalp EEG Database, version 1.0.0, PhysioNet. doi:10.13026/5d4a-j060. Database documentation: https://physionet.org/content/siena-scalp-eeg/1.0.0/.

[2] MathWorks. CWT filter bank scale spectrum: wavelet-energy normalization and the admissibility constant. https://www.mathworks.com/help/wavelet/ref/cwtfilterbank.scalespectrum.html (accessed 12 September 2026).

[3] Jirsa VK, Stacey WC, Quilichini PP, Ivanov AI, Bernard C. On the nature of seizure dynamics. Brain. 2014 Aug;137(Pt 8):2210-30. doi: 10.1093/brain/awu133. Epub 2014 Jun 11. PMID: 24919973; PMCID: PMC4107736.

Supplementary Figures

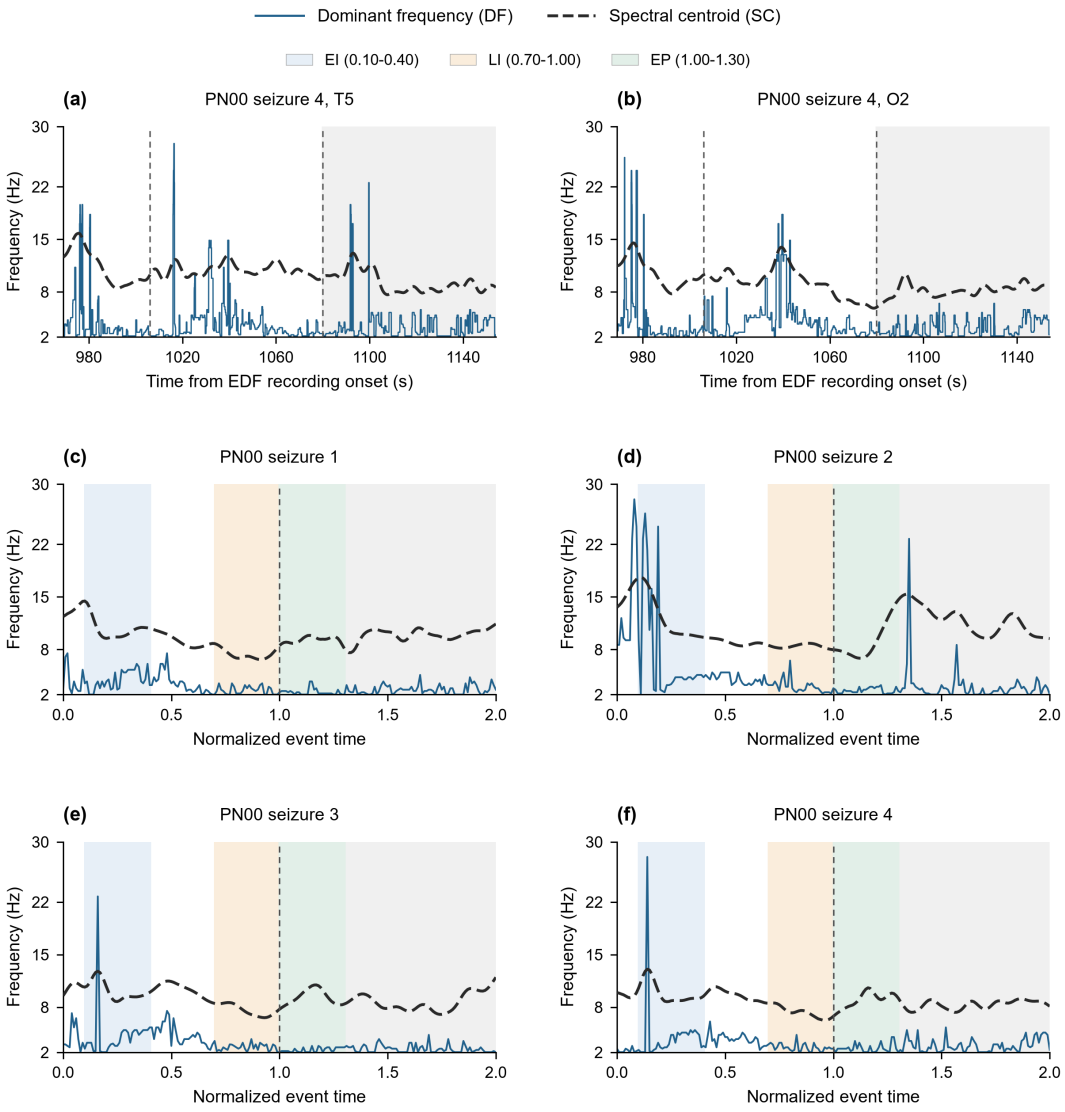


Figure S1. Dominant frequency in Patient PN00

(a,b) CWT-derived dominant frequency (DF, blue) and spectral centroid (SC, dashed black) for T5 and O2 during PN00 seizure 4, corresponding to main-text Figure 2. The horizontal axes show seconds from EDF recording onset; dashed vertical lines mark seizure onset and offset. (c-f) Event-level DF and SC trajectories for PN00 seizures 1-4, respectively. Each feature is summarized as the pointwise median across eligible EEG channels. Onset, offset, and the analysis endpoint correspond to normalized times 0, 1, and 2. Gray shading denotes the analyzed postictal interval. Pale blue, orange, and green shading in (c-f) marks the early ictal (EI, 0.10-0.40), late ictal (LI, 0.70-1.00), and early postictal (EP, 1.00-1.30) comparison windows, respectively. All measures use linear CWT power within 2-30 Hz. SC curves in (a,b) reproduce those in main-text Figure 2(d), and SC curves in (c-f) match the corresponding event curves in Figure 3(a). SC received additional approximately 10-s Gaussian smoothing for display only; slopes and phase comparisons use the analytical trajectories before this additional smoothing. DF retains the analytical moving-median filtering described in Section S2.2 without additional display smoothing. Event-level effects and descriptive uncertainty are reported in Table S3. CWT, continuous wavelet transform.

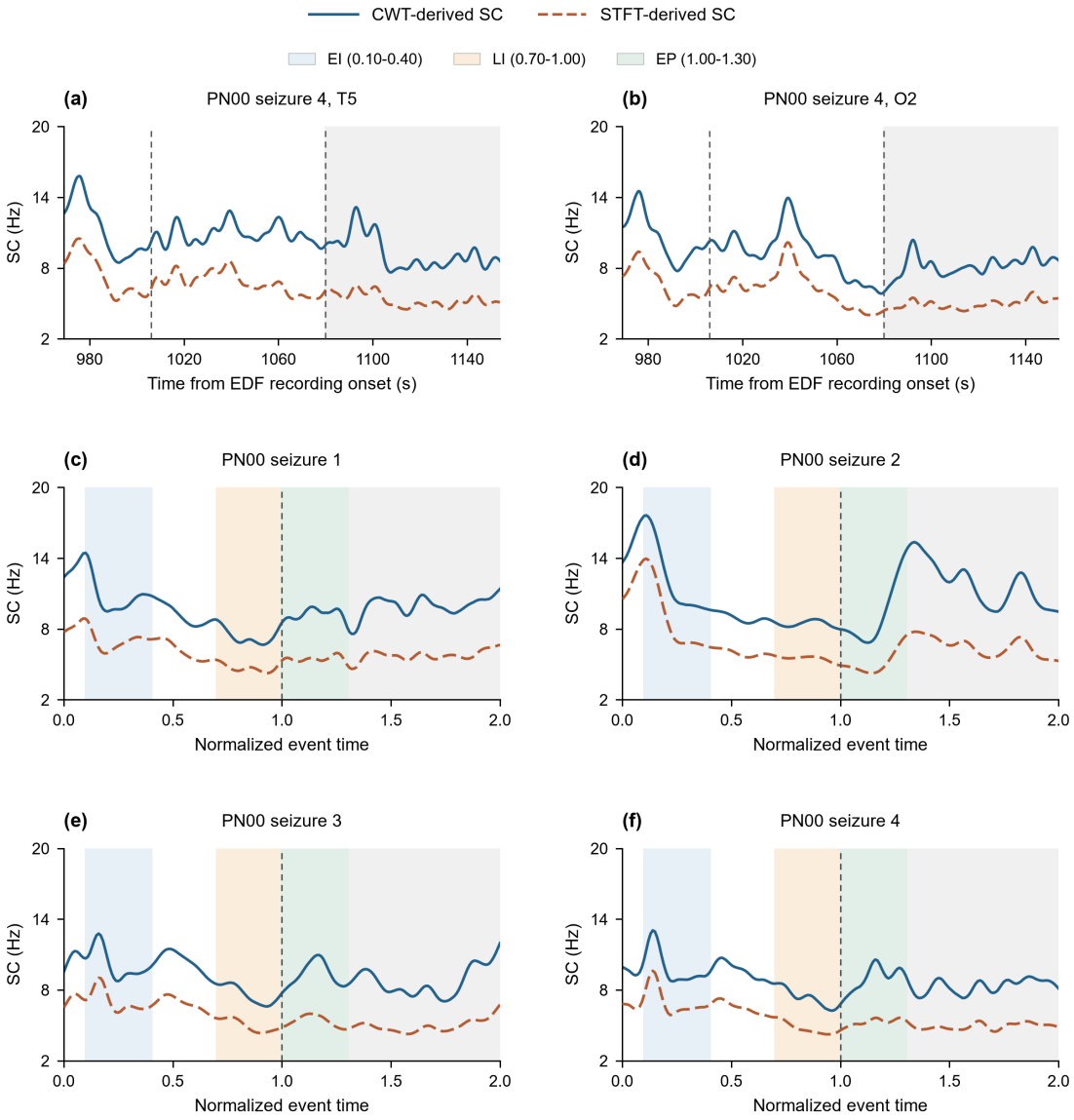


Figure S2. CWT and STFT comparison of spectral centroid in Patient PN00

(a,b) SC trajectories for T5 and O2 during PN00 seizure 4, corresponding to main-text Figure 2. (c-f) Event-level SC for PN00 seizures 1-4, respectively, each summarized as the pointwise median across eligible EEG channels. Solid blue and dashed orange curves are calculated from CWT and STFT linear power, respectively, using the same 2-30 Hz analysis range. Panels (a,b) retain seconds from EDF recording onset, with dashed lines marking onset and offset; panels (c-f) use normalized time, with onset at 0 and offset at 1. Gray shading denotes the analyzed postictal interval. Pale blue, orange, and green shading in (c-f) marks the early ictal (EI, 0.10-0.40), late ictal (LI, 0.70-1.00), and early postictal (EP, 1.00-1.30) comparison windows, respectively. CWT curves reuse those in main-text Figures 2(d) and 3(a). Both transforms receive approximately 10-s Gaussian display smoothing; slopes and phase comparisons use the analytical trajectories before this additional smoothing. SC, spectral centroid; CWT, continuous wavelet transform; STFT, short-time Fourier transform.

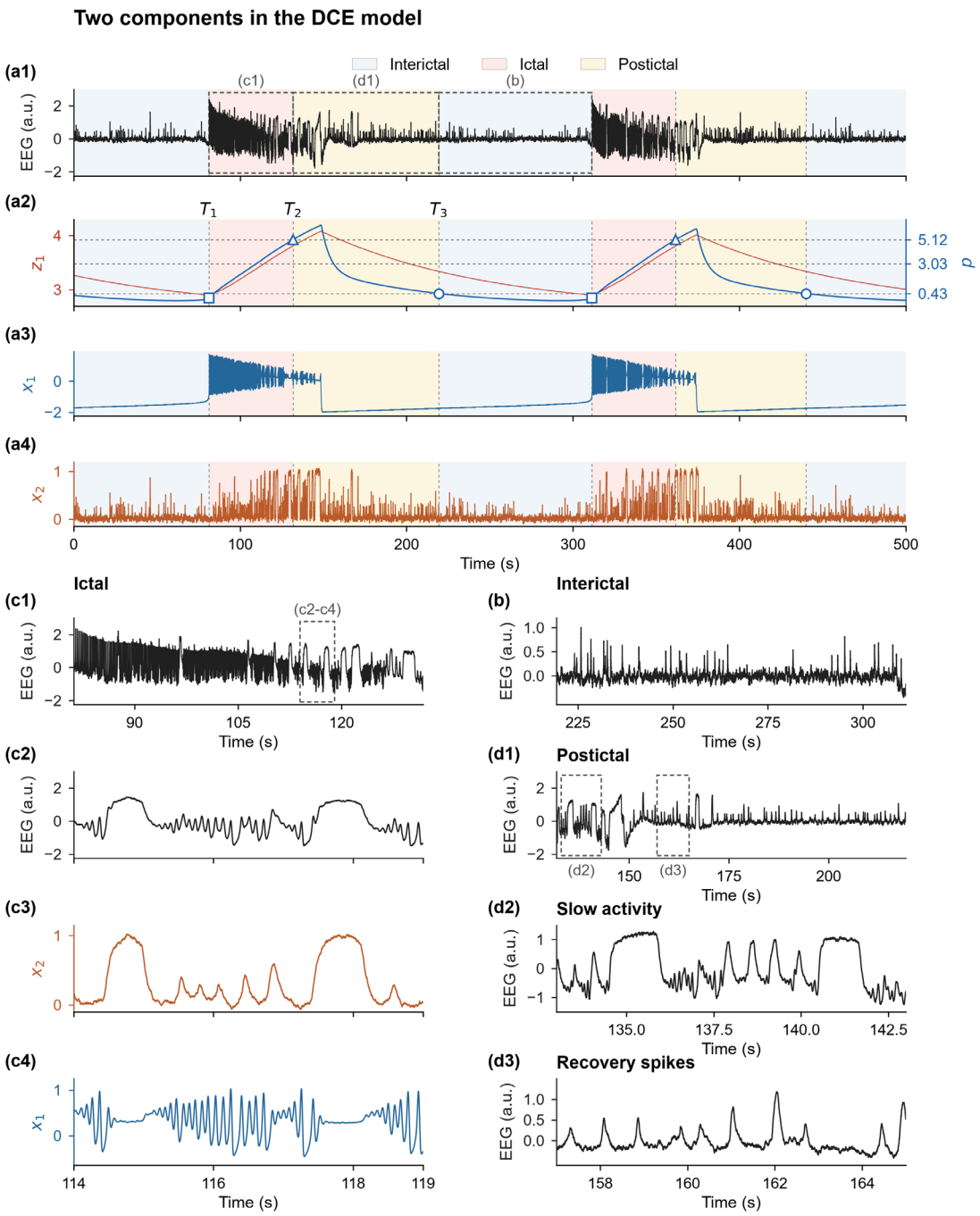


Figure S3. Model phases, waveform evolution, and subsystem interaction.

(a1-a4) EEG, z_1 (red, left) and p (blue, right), x_1, and x_2. Shading identifies the three model phases. The square marks T_1; the triangle and circle mark the upward wave-threshold and downward spike-threshold crossings (T_2 and T_3). (b) Complete interictal interval after the first event (219.4-311.3 s). (c1) Ictal EEG. (c2-c4) Aligned EEG, x_2, and x_1 at 114-119 s. (d1) Postictal EEG. (d2,d3) Slow activity at 133-143 s and recovery spikes at 157-165 s. Dashed boxes locate the enlarged windows. Times share the simulation axis; state variables are dimensionless.

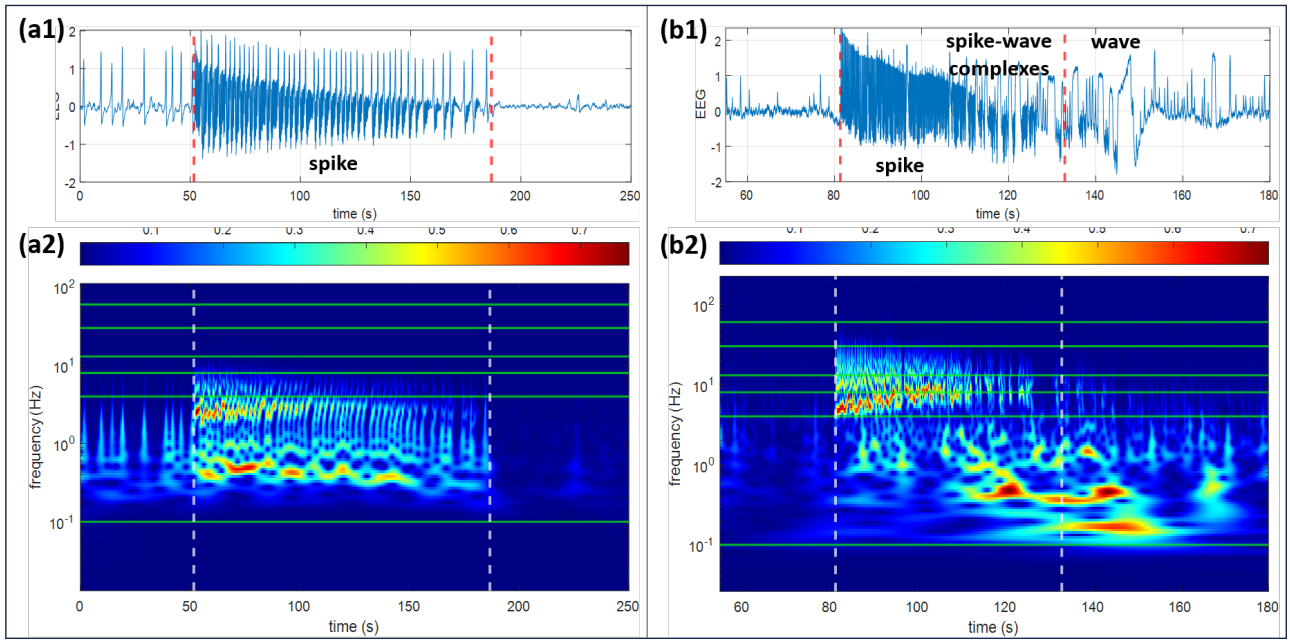


Figure S4. Qualitative comparison of seizure-like events generated by the Epileptor and DCE models.

(a1,a2) Simulated EEG and corresponding continuous wavelet transform (CWT) spectrogram for the original Epileptor model [3]. (b1,b2) Corresponding results for the DCE model. The simulations illustrate the waveform and spectral evolution discussed in Section S4.

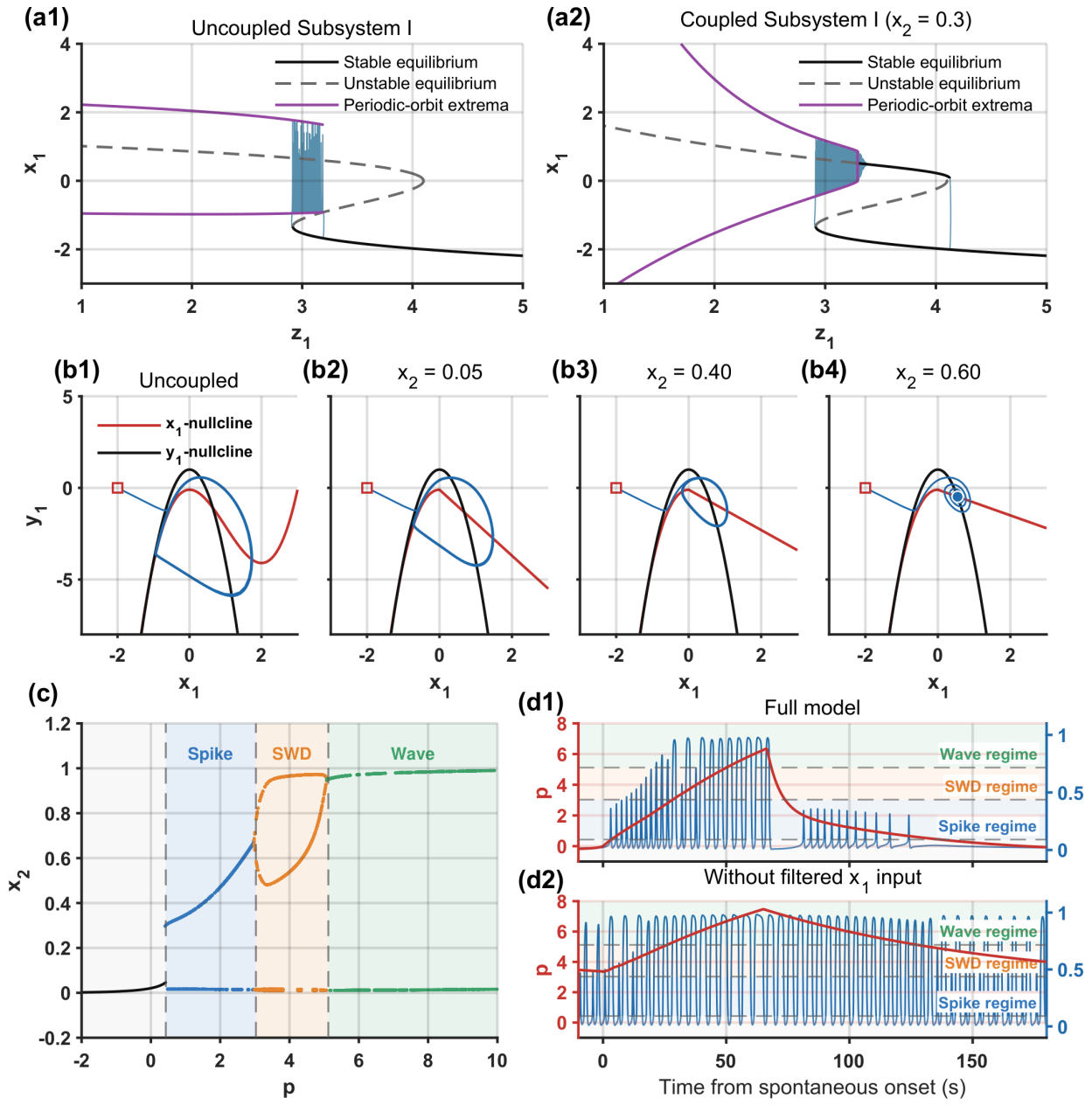


Figure S5. Controlled comparisons of subsystem and coupling contributions.

(a) Bifurcation structure of Subsystem I using the original cubic nonlinearity (a1) or the coupled nonlinearity at fixed x2 = 0.30 (a2). Solid black and dashed gray curves denote stable and unstable equilibria, purple curves periodic-orbit extrema, and blue traces sample trajectories. (b) Fast-subsystem phase portraits at z1 = 3 using the original cubic form (b1) and the coupled form at x2 = 0.05, 0.40, and 0.60 (b2-b4). Red and black curves are the x1 and y1 nullclines; blue curves are trajectories. (c) Subsystem II extrema of x2 versus p, with spike, spike-wave discharge (SWD), and wave regimes and their threshold lines. (d) Full-model (d1) and filtered-input-removal (d2) trajectories. The left red axis is p and the right blue axis is x2; time is measured from the respective burst onset. State variables and p are dimensionless. Noise is disabled throughout these controls.

Supplementary Tables

Table S1. Participant and event inclusion summary

Patient	Age	Sex	Type	Region/side	Eligible/all events	Channels/event
PN00	55	Male	IAS	T/R	4/5	29
PN01	46	Male	IAS	T/L	0/2	-
PN03	54	Male	IAS	T/R	2/2	29
PN05	51	Female	IAS	T/L	1/3	29
PN06	36	Male	IAS	T/L	4/5	29
PN07	20	Female	IAS	T/L	1/1	29
PN09	27	Female	IAS	T/L	0/3	-
PN10	25	Male	FBTC	F/Bilateral	10/10	18-19
PN11	58	Female	IAS	T/R	0/1	-
PN12	71	Male	IAS	T/L	4/4	29
PN13	34	Female	IAS	T/L	2/3	29
PN14	49	Male	WIAS	T/L	2/4	29
PN16	41	Female	IAS	T/L	2/2	29
PN17	42	Male	IAS	T/R	1/2	29

Patient metadata are reproduced from the database subject-information file. IAS, focal onset impaired-awareness seizure; WIAS, focal onset without impaired awareness; FBTC, focal-to-bilateral tonic-clonic seizure; T, temporal; F, frontal; L, left; R, right. Eligible/all events refers to the 2-30 Hz nominal-passband criterion. PN10 had 19 EEG channels; one channel failed the passband criterion in the recording containing seizures 4-6, leaving 18 eligible channels for these events.

Table S2. Event-level timing, passband, and eligibility

Patient/event	EDF file	Onset (s)	Offset (s)	D (s)	HP	LP	Ch.	Status
PN00/1	PN00-1	1143	1213	70	1.59155	30	29	Included
PN00/2	PN00-2	1220	1274	54	1.59155	30	29	Included
PN00/3	PN00-3	765	825	60	1.59155	30	29	Included
PN00/4	PN00-4	1006	1080	74	1.59155	30	29	Included
PN00/5	PN00-5	904	971	67	5.30516	30	-	Excluded: HP >=2
PN01/1	PN01-1	10218	10272	54	5.30516	30	-	Excluded: HP >=2
PN01/2	PN01-1	46353	46427	74	5.30516	30	-	Excluded: HP >=2
PN03/1	PN03-1	38673	38784	111	0.530516	30	29	Included
PN03/2	PN03-2	34921	35054	133	1.59155	30	29	Included
PN05/2	PN05-2	7163	7198	35	1.59155	30	29	Included
PN05/3	PN05-3	6836	6866	30	1.59155	15	-	Excluded: LP <30
PN05/4	PN05-4	3608	3647	39	1.59155	15	-	Excluded: LP <30
PN06/1	PN06-1	5583	5647	64	1.59155	15	-	Excluded: LP <30
PN06/2	PN06-2	8860	8929	69	0.530516	30	29	Included
PN06/3	PN06-3	6275	6317	42	1.59155	30	29	Included
PN06/4	PN06-4	5939	6002	63	1.59155	30	29	Included
PN06/5	PN06-5	4783	4827	44	1.59155	30	29	Included
PN07/1	PN07-1	22059	22121	62	1.59155	30	29	Included
PN09/1	PN09-1	7249	7329	80	0.530516	15	-	Excluded: LP <30
PN09/2	PN09-2	7127	7186	59	1.59155	15	-	Excluded: LP <30
PN09/3	PN09-3	7221	7285	64	5.30516	15	-	Excluded: HP >=2, LP <30
PN10/1	PN10-1	7545	7614	69	1.59155	30	19	Included
PN10/2	PN10-2	7798	7849	51	1.59155	30	19	Included
PN10/3	PN10-3	7835	7904	69	0.530516	30	19	Included
PN10/4	PN10-4.5.6	2309	2314	5	0.159155	50;15	18	Included (1 ch. omitted)
PN10/5	PN10-4.5.6	6544	6563	19	0.159155	50;15	18	Included (1 ch. omitted)
PN10/6	PN10-4.5.6	11225	11282	57	0.159155	50;15	18	Included (1 ch. omitted)
PN10/7	PN10-7.8.9	2748	2796	48	1.59155	50	19	Included
PN10/8	PN10-7.8.9	5459	5477	18	1.59155	50	19	Included
PN10/9	PN10-7.8.9	12923	12938	15	1.59155	50	19	Included
PN10/10	PN10-10	7977	7991	14	1.59155	50	19	Included
PN11/1	PN11-1	7554	7609	55	0.530516	15	-	Excluded: LP <30
PN12/1	PN12-1.2	1312	1375	63	1.59155	30	29	Included
PN12/2	PN12-1.2	9570	9638	68	1.59155	30	29	Included
PN12/3	PN12-3	772	868	96	1.59155	30	29	Included
PN12/4	PN12-4	9812	9875	63	1.59155	30	29	Included

Patient/event	EDF file	Onset (s)	Offset (s)	D (s)	HP	LP	Ch.	Status
PN13/1	PN13-1	7062	7110	48	1.59155	30	29	Included
PN13/2	PN13-2	7249	7314	65	1.59155	15	-	Excluded: LP <30
PN13/3	PN13-3	7553	7704	151	0.530516	30	29	Included
PN14/1	PN14-1	7262	7289	27	1.59155	15	-	Excluded: LP <30
PN14/2	PN14-2	7479	7491	12	1.59155	30	29	Included
PN14/3	PN14-3	17540	17581	41	1.59155	15	-	Excluded: LP <30
PN14/4	PN14-4	5463	5546	83	1.59155	30	29	Included
PN16/1	PN16-1	7184	7307	123	1.59155	30	29	Included
PN16/2	PN16-2	8574	8681	107	1.59155	30	29	Included
PN17/1	PN17-1	8420	8490	70	1.59155	30	29	Included
PN17/2	PN17-2	7731	7814	83	1.59155	15	-	Excluded: LP <30

Onset and offset are seconds from EDF recording onset; **HP and LP are nominal high-pass and low-pass cutoffs in Hz from the EDF metadata**. PN00 event 3 uses 18:29:29 (825 s) as the author-inferred offset because the listed 19:29:29 time lies outside the EDF recording. The source file was not altered.

Table S3. Individual-seizure effects and descriptive uncertainty in Patient PN00

Measure	Event / summary	Ictal slope	Late ictal minus early ictal	Early postictal minus early ictal	Full-window slope
SC	1	-6.285	-3.398	-1.361	-0.417
SC	2	-7.818	-3.649	-3.043	-0.354
SC	3	-4.128	-2.557	-0.819	-0.902
SC	4	-4.208	-2.765	-0.855	-0.889
SC	Mean	-5.610	-3.093	-1.520	-0.640
SC	SD	1.779	0.515	1.045	0.296
SC	Bootstrap 95% interval for the mean	[-7.052, -4.168]	[-3.524, -2.661]	[-2.496, -0.837]	[-0.895, -0.385]
MF	1	-6.306	-3.047	-1.539	-1.350
MF	2	-10.228	-4.614	-3.835	-0.703
MF	3	-3.636	-2.354	-1.693	-1.712
MF	4	-4.422	-3.245	-1.715	-1.591
MF	Mean	-6.148	-3.315	-2.196	-1.339
MF	SD	2.942	0.946	1.096	0.450
MF	Bootstrap 95% interval for the mean	[-8.776, -4.029]	[-4.222, -2.576]	[-3.300, -1.583]	[-1.651, -0.925]
LFR	1	0.295	0.155	0.126	0.070
LFR	2	0.472	0.205	0.223	0.061
LFR	3	0.177	0.112	0.087	0.102
LFR	4	0.214	0.155	0.111	0.111
LFR	Mean	0.289	0.157	0.137	0.086
LFR	SD	0.131	0.038	0.060	0.024
LFR	Bootstrap 95% interval for the mean	[0.195, 0.407]	[0.123, 0.193]	[0.097, 0.195]	[0.065, 0.107]

Measure	Event / summary	Ictal slope	Late ictal minus early ictal	Early postictal minus early ictal	Full-window slope
DF	1	-1.844	-1.376	-1.614	-0.781
DF	2	-10.500	-4.015	-4.508	-3.416
DF	3	-1.981	-1.569	-1.922	-1.245
DF	4	-1.208	-1.547	-1.658	-0.496
DF	Mean	-3.883	-2.127	-2.426	-1.484
DF	SD	4.424	1.262	1.395	1.324
DF	Bootstrap 95% interval for the mean	[-8.336, -1.401]	[-3.398, -1.425]	[-3.795, -1.636]	[-2.757, -0.639]

Ictal and full-window slopes are least-squares estimates over normalized times 0-1 and 0-2, respectively, expressed per normalized-time unit. Changes compare late ictal (0.70-1.00) or early postictal (1.00-1.30) with early ictal (0.10-0.40) window means. SC, MF, and DF changes are in Hz; LFR changes are absolute fractions. SD describes variation across the four events. Bootstrap 95% intervals describe uncertainty in the within-patient mean using the 2.5th and 97.5th percentiles of all 256 size-four resamples with replacement. Whole events, not time points or channels, are resampled. These exploratory intervals are conditional on four exchangeable events from PN00 and do not account for possible temporal dependence between events. They are intervals for mean effects, not confidence bands around individual trajectories or confidence intervals for each event. Calculations use the analytical trajectories before the additional display smoothing.

Table S4. Multi-patient statistical analysis of ictal and early postictal spectral changes

CWT descriptors

Measure	Endpoint	Median	95% CI	P	Q	-/+
SC_CWT	Ictal slope	-0.961	[-2.705, 0.321]	0.2061	0.2820	7/4
SC_CWT	LI-EI	-0.311	[-1.110, 0.957]	0.5771	0.6125	7/4
SC_CWT	EP-EI	1.560	[-0.548, 3.863]	0.0420	0.1040	3/8
SC_CWT	Full slope	0.961	[-0.640, 2.176]	0.0420	0.1040	3/8
MF_CWT	Ictal slope	-0.589	[-3.955, 1.212]	0.4131	0.4773	6/5
MF_CWT	LI-EI	-0.331	[-1.325, 2.404]	0.8984	0.8984	6/5
MF_CWT	EP-EI	2.188	[-1.175, 4.538]	0.0830	0.1660	3/8
MF_CWT	Full slope	1.133	[-1.026, 2.656]	0.1230	0.2000	3/8
LFR_CWT	Ictal slope	0.056	[-0.027, 0.166]	0.0674	0.1402	4/7
LFR_CWT	LI-EI	0.034	[-0.058, 0.076]	0.5195	0.5748	5/6
LFR_CWT	EP-EI	-0.073	[-0.187, 0.003]	0.1016	0.1821	8/3
LFR_CWT	Full slope	-0.071	[-0.117, 0.079]	0.2061	0.2820	8/3
DF_CWT	Ictal slope	-1.327	[-2.679, 0.177]	0.0322	0.0931	8/3
DF_CWT	LI-EI	-1.002	[-1.451, -0.370]	0.0186	0.0568	9/2
DF_CWT	EP-EI	0.278	[-1.346, 6.019]	0.3203	0.3966	4/7
DF_CWT	Full slope	0.418	[-1.157, 0.909]	0.7646	0.7952	5/6

STFT descriptors

Measure	Endpoint	Median	95% CI	P	Q	-/+
SC_STFT	Ictal slope	-1.184	[-2.671, 0.272]	0.1748	0.2597	7/4
SC_STFT	LI-EI	-0.356	[-1.485, 0.451]	0.3652	0.4417	6/5
SC_STFT	EP-EI	1.280	[-1.168, 3.156]	0.2061	0.2820	4/7
SC_STFT	Full slope	0.646	[-1.222, 1.305]	0.4648	0.5255	4/7
MF_STFT	Ictal slope	-0.966	[-2.681, 0.217]	0.0674	0.1402	7/4
MF_STFT	LI-EI	-0.442	[-1.453, 0.234]	0.1475	0.2324	7/4
MF_STFT	EP-EI	0.862	[-1.553, 4.417]	0.4131	0.4773	4/7
MF_STFT	Full slope	0.589	[-0.901, 0.825]	0.8984	0.8984	5/6
LFR_STFT	Ictal slope	0.062	[-0.017, 0.178]	0.0420	0.1040	4/7
LFR_STFT	LI-EI	0.022	[-0.038, 0.117]	0.3203	0.3966	5/6
LFR_STFT	EP-EI	-0.061	[-0.160, 0.045]	0.1748	0.2597	7/4
LFR_STFT	Full slope	-0.064	[-0.089, 0.092]	0.5771	0.6125	7/4

Absolute STFT power

Measure	Endpoint	Median	95% CI	P	Q	-/+
LowPower	Ictal slope	8.191	[0.826, 14.133]	0.0137	0.0508	2/9
LowPower	LI-EI	2.391	[-1.260, 6.617]	0.1016	0.1821	4/7
LowPower	EP-EI	-5.156	[-8.324, -2.012]	0.0049	0.0317	10/1
LowPower	Full slope	-3.123	[-5.222, -2.425]	0.0010	0.0127	11/0
HighPower	Ictal slope	2.538	[-0.013, 7.864]	0.0674	0.1402	3/8
HighPower	LI-EI	1.451	[-0.747, 3.178]	0.2402	0.3203	4/7
HighPower	EP-EI	-2.152	[-5.330, -0.843]	0.0098	0.0423	9/2
HighPower	Full slope	-2.836	[-5.259, -1.169]	0.0068	0.0323	10/1
TotalPower	Ictal slope	6.555	[1.352, 11.546]	0.0186	0.0568	2/9
TotalPower	LI-EI	2.403	[-1.007, 6.370]	0.1016	0.1821	4/7
TotalPower	EP-EI	-3.206	[-5.175, -2.232]	0.0049	0.0317	9/2
TotalPower	Full slope	-2.833	[-5.357, -1.726]	0.0010	0.0127	11/0

Absolute CWT power

Measure	Endpoint	Median	95% CI	P	Q	-/+
LowPower	Ictal slope	7.908	[0.715, 13.305]	0.0137	0.0508	2/9
LowPower	LI-EI	2.302	[-1.308, 6.416]	0.1230	0.2000	4/7
LowPower	EP-EI	-5.341	[-8.895, -2.008]	0.0049	0.0317	10/1
LowPower	Full slope	-3.228	[-5.380, -2.385]	0.0010	0.0127	11/0
HighPower	Ictal slope	2.373	[-0.106, 7.732]	0.0537	0.1270	3/8
HighPower	LI-EI	1.272	[-1.386, 3.328]	0.2783	0.3618	4/7
HighPower	EP-EI	-2.557	[-5.261, -0.771]	0.0068	0.0323	9/2
HighPower	Full slope	-3.276	[-5.608, -1.403]	0.0068	0.0323	10/1
TotalPower	Ictal slope	6.919	[0.955, 11.366]	0.0186	0.0568	2/9
TotalPower	LI-EI	2.494	[-1.029, 6.282]	0.1230	0.2000	4/7
TotalPower	EP-EI	-3.248	[-5.175, -2.402]	0.0049	0.0317	9/2
TotalPower	Full slope	-3.114	[-5.318, -1.825]	0.0010	0.0127	11/0

EI, early ictal; LI, late ictal; EP, early postictal; **-/+, numbers of patient-level effects below/above zero**. Median and 95% CI describe the patient-level effect distribution and the bootstrap interval for its median. P is the unadjusted two-sided test result; Q is the Benjamini-Hochberg-adjusted P value across the 52-test family. Frequency changes use Hz, LFR changes are dimensionless, and absolute-power changes use dB; slopes are expressed per normalized-time unit. LowPower, HighPower, and TotalPower refer to 2-8, 8-30, and 2-30 Hz, respectively. These analyses are exploratory.

Table S5. Late-trajectory peak-to-peak amplitude of x1 in the fixed-z1 fast-subsystem controls of Figure S5(b).

Configuration	Fixed x2	Peak-to-peak x1
Original cubic f1	Not applicable	2.675
Coupled f1	0.05	2.187
Coupled f1	0.40	1.235
Coupled f1	0.60	< 10^-12

All quantities are dimensionless. These values describe deterministic trajectories, not replicate means or statistical estimates.